Retrieving Soil Moisture Over Soybean Fields During Growing Season Through Polarimetric Decomposition

Tengfei Xiao, Minfeng Xing, Binbin He, Jinfei Wang, *Member, IEEE*, Jiali Shang, *Member, IEEE*, Xiaodong Huang, and Xiliang Ni

***Abstract*—Soil moisture (*Mv*) estimation and monitoring over agricultural areas using Synthetic Aperture Radar (SAR) are often affected by vegetation cover during the growing season. Volume scattering and vegetation attenuation can complicate the received SAR backscatter signal when microwave interacts with the vegetation canopy. To address the existing problems, this article employed the model-based polarimetric decomposition method considering the two-way attenuation to remove the volume scattering and vegetation attenuation. A deorientation process of SAR data was applied to remove the influence of randomly distributed target orientation angles before the polarimetric decomposition. To parameterize the two-way attenuation, Radar Vegetation Index derived from the SAR intensity images was adopted. The Dubois model was used to describe backscattering from the underlying bare soil. Since the soil roughness parameters are difficult to measure under vegetation cover, the optimum surface roughness method was used to parameterize the Dubois model. This soil moisture retrieval algorithm was applied to the polarimetric multitemporal RADARSAT-2 SAR data over soybean fields. The validation indicates the root-mean-square error of 9.2 vol.% and 8.2 vol.% at HH and VV polarization, respectively, over the entire soybean growing period, suggesting that the proposed method is capable of reducing the effect of vegetation cover for soil moisture monitoring over the soybean field.**

***Index Terms*—Deorientation process, Dubois model, optimal surface roughness, polarimetric decomposition, soil moisture, vegetation attenuation.**

Manuscript received January 17, 2020; revised June 9, 2020 and September 22, 2020; accepted November 17, 2020. Date of publication December 2, 2020; date of current version January 6, 2021. This research was supported by Sichuan Science and Technology Program, under Grant 2020YFG0048, and Grant 2020YFS0058, in part by the National Natural Science Foundation of China, under Grant 41601373, in part by the Open Fund of State Key Laboratory of Remote Sensing Science, under Grant OF SLRSS201712, in part by the Fundamental Research Funds for the Central Universities under Grant ZYGX2019J070, and in part by the Canadian Space Agency SOAR-E program under Grant SOAR-E-5489. The field campaign was funded by NSERC discovery grant awarded to Jinfei Wang and Agricultural and Agri-Food Canada A-base Project No. 1130. *(Corresponding authors: Minfeng Xing; Binbin He.)*

Tengfei Xiao is with the School of Resources and Environment, University of Electronic Science and Technology of China, Chengdu 611731, China (e-mail: 201821070210@std.uestc.edu.cn).

Minfeng Xing and Binbin He are with the School of Resources and Environment, University of Electronic Science and Technology of China, Chengdu 611731, China, and also with the Center for Information and Geoscience, University of Electronic Science and Technology of China, Chengdu 611731, China (e-mail: xingminfeng@uestc.edu.cn; binbinhe@uestc.edu.cn).

Jinfei Wang is with the University of Western Ontario, London, ON N6A5C2, Canada (e-mail: jfwang@uwo.ca).

Jiali Shang is with Agriculture and Agri-Food Canada, Ottawa, ON K1A0C6, Canada (e-mail: jiali.shang@canada.ca).

Xiaodong Huang is with the Applied Geosolutions, Durham, NH 03824 USA (e-mail: rs.xiaodong@gmail.com).

Xiliang Ni is with the State Key Laboratory of Remote Sensing Science, Institute of Remote Sensing and Digital Earth, Chinese Academy of Sciences, Beijing 100101, China (e-mail: nixl@radi.ac.cn).

Digital Object Identifier 10.1109/JSTARS.2020.3041828

I. Introduction

SOIL moisture (*Mv*) is a crucial factor in many applications such as agriculture, environment, hydrology, ecology, and water management [1]–[6]. For example, soil moisture greatly governs crop growth and nutrient uptake, which in turn affects the final crop yield [7], [8]. Traditionally, the soil moisture is measured by *in situ* field campaign, which is very time-consuming and difficult to carry on over a large area. Remote sensing provides an effective method to estimate and monitor soil moisture at different spatial and temporal scales [7], [9], [10]. Particularly, due to the penetration ability and high sensitivity to soil moisture, synthetic aperture radar (SAR) has been widely used for soil moisture retrieval at high spatial and temporal resolution [11], [12].

The study of soil moisture estimation has been ongoing for decades and can be divided into two categories: soil moisture retrieval over bare soil and under vegetation cover. Over bare soil, the backscatter signal received by the SAR sensor is determined by surface parameters (surface roughness, soil moisture, etc.). To retrieve soil moisture over bare soil, several models such as Oh, Dubois, and IEM have been proposed with desirable results since the last century [13]–[15]. The soil moisture retrieval over bare soil depends on the measurement of soil surface roughness. However, soil surface roughness parameters are difficult to measure accurately due to measurement technique [16] and profile length [17]. Furthermore, dense vegetation cover during peak growing season can also obstruct soil roughness measurements. Several studies have focused on developing new algorithms to avoid *in situ* measured soil roughness parameters [2], [18]–[20]. Su *et al*. proposed the calibrated (effective) roughness parameters [20], which used the estimated surface roughness parameters from previous acquisitions to derive the radar backscatter models for subsequent SAR data analysis [20]. In 2016, Bai *et al*. [9] proposed the optimal roughness parameters, in which roughness parameters having the best-retrieved soil moisture were selected as the optimal ones, and a desirable retrieved soil moisture was achieved [9].

Over vegetated areas like agricultural field, SAR backscattering signal is more complex than that of bare soils due to vegetation effect [7], where it mainly affects SAR backscattering signal in two ways. First, when the microwave signal passes through vegetation canopy, volume scattering will be mixed into the received total backscatter signal leading to an increase of the total backscattering power [21], [22]. In addition, vegetation water content (VWC) of the crop canopy also attenuates the SAR signal [23], [24], which will decrease the received backscattering power [25].

In general, primary algorithms used for soil moisture retrieval under vegetation cover are microwave radiation transfer model (RTM) and polarimetric SAR (PolSAR) decomposition. Early studies of soil moisture retrieval under vegetation cover are mainly concentrated on RTM [26]–[30]. Among the RTMs, the semi-physical classical water cloud model (WCM) is extensively used, which assumes that vegetation consists of a collection of spherical water droplets that are structurally held in place by dry matter [26]. The received total backscatter coefficient is modeled as the summation of the contributions from the vegetation canopy, the attenuated underlying soil contribution, and the double-bounce backscatter caused by the interaction between vegetation and soil. With the advancement of SAR sensors, PolSAR shows increasing potential for soil moisture retrieval due to the rich dielectric and crop structural information captured by the full polarization signal [23]. However, the retrieval of soil moisture through RTMs under vegetation cover rarely incorporates the polarimetric properties, limiting the interpretation of the PolSAR signals.

Apart from retrieving through RTMs, soil moisture can also be estimated using the polarimetric model-based decomposition, which is a powerful method to interpret PolSAR signal compositions. Hajnsek *et al*. first investigated the potential of the model-based decomposition on soil moisture retrieval under different crop covers at L-band [21]. In their study, the soil moisture was derived from both surface scattering component by the X-Bragg model and dihedral scattering component by the Fresnel model. However, due to different scattering properties and penetration ability between L-band and C-band SAR, the L-band polarimetric decomposition method might not be valid for C-band SAR data [24]. To retrieve soil moisture through polarimetric decomposition at C-band, the X-Bragg model in the L-band polarimetric decomposition method was replaced by surface scattering models (IEM, Oh, etc.) in several studies [24], [31]. Wang *et al*. considered the vegetation attenuation at C-band and neglected the dihedral scattering component, which has greatly simplified the soil moisture retrieval using the polarimetric decomposition [24].

In this study, the model-based polarimetric decomposition method was used to remove the vegetation volume scattering. Compared with L-band, the dihedral scattering component of C-band is rather weak over soybean fields. Thus, the same strategy proposed in [24] was adopted in this study, where the dihedral scattering was omitted. The deorientation process [32] of SAR data was applied before polarimetric decomposition to remove the influence of randomly distributed target orientation angles and overestimation of the volume scattering component. The vegetation attenuation effect was modeled through a two-way attenuation parameter described used in the WCM [26]. Compared with parameterizing the vegetation attenuation using optical vegetation indices such as VWC, leaf area index (LAI), etc., the radar vegetation index (RVI) derived from SAR itself was used in this study, which avoids the dependence on prior optical vegetation indices. After the removal of volume scattering, the Dubois model [14] was used to describe the backscattering of the underlying soil for the following reasons. First, the desirable validity range ($\mathrm{m_v} < 35$ vol.%, $k{\cdot}s < 2.5$, $\theta > 30°$) of the Dubois model covers a large range of soil moisture and roughness conditions over agricultural fields in the temperate climate zone [14]. Second, compared with the Oh, IEM model, etc., the relationship between soil dielectric constant and SAR backscatter coefficient is reversible; through which soil moisture can be derived directly by the dielectric constant models [33], [34]. Since the soil surface roughness parameters greatly affect the soil moisture retrieval due to the difficulty in getting precise measurements, the optimal surface roughness method proposed by Bai *et al*. [9] was used in this study to parameterize the Dubois model. Multitemporal RADARSAT-2 images together with *in situ* soil moisture measurement over soybean fields in southwest Canada were used for validation.

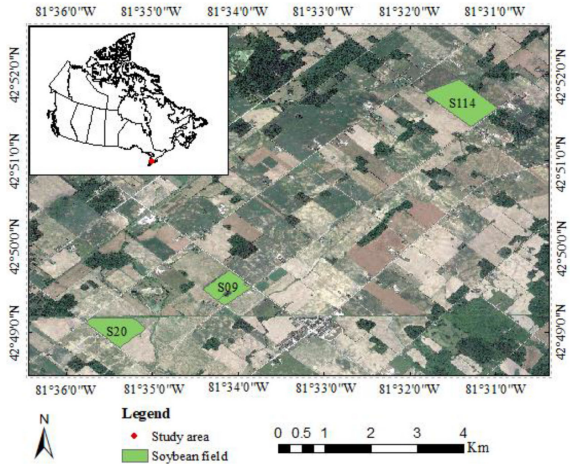

Fig. 1. Location of the study area and soybean fields. The background image is from Google Earth.

The rest of the article is structured as follows. Section II introduces the study area and data including *in situ* measured soil moisture and time-series RADARSAT-2 images. Sections III and IV describe the proposed soil moisture retrieval method. Results and discussion are presented in Section V. Conclusions are given in Section VI.

II. Study Site and Data Collection

A. In Situ Soil Moisture Data Collection

An agriculturally productive area was selected as the study site, which is located near London in southwestern Ontario, Canada (see Fig. 1). Major crops in this region include soybean, winter wheat, and corn. In this study, only soybean fields were used for model development and validation. Soybean in this area is rain-fed and sown in May and harvested in late September or early October. Fig. 2 shows ground truth photos of soybean. The terrain of the soybean fields is generally flat and only about a

Fig. 2. Ground truth photos of soybean on (a) July 17, (b) August 10, (c) September 13, (d) October 1.

TABLE I
COLLECTED SOIL MOISTURE

Acquired Date	Sample Sites Amount (S09)	Sample Sites Amount (S20)	Sample Sites Amount (S114)	Total Sites Amount	Soil Moisture Range (vol.%)	BBCH	Vegetation Coverage (%)
2015.07.17	8	8	8	24	14.0~38.3	51	41.1~61.7
2015.08.10	8	8	8	24	12.0~34.7	70	58.8~87.3
2015.09.03	4	4	3	11	4.3~31.0	78	46.1~76.9
2015.09.13	8	8	8	24	9.5~21.8	82	50.6~64.4
2015.09.17	8	8	8	24	7.0~18.6	87	40.1~50.0
2015.09.27	0	8	8	16	4.3~15.1	97	27.8~34.4
2015.10.01	8	8	8	24	7.5~26.3	99	19.5~24.5

quarter of the land is on a gentle slope. Ground measurements were taken by the team members of Geographic Technology and Application Laboratory at the University of Western Ontario during the 2015 growing season. Field campaign was conducted throughout the soybean growth period close to the RADARSAT-2 satellite overpassing time. In this study, a total of three soybean fields (namely S09, S20, S114, respectively) shown in Fig. 1 were selected for model validation. The distance between every two fields is more than 2 km. A total of seven campaigns paired with concurrent RADARSAT-2 data acquisition from July 2015 to October 2015 were used for validation. Within each field, three to eight sample sites were selected to capture the within-field soil moisture variability, resulting in 11 to 24 samples per satellite acquisition and a total of 147 samples for the entire season. During the field campaign, each sample site was placed at least 50 m apart from the other sites to avoid spatial correlation.

During the field campaign, several parameters including vegetation cover fraction, plant area index (PAI), and the BBCH (Biologische Bundesantalt, Bundessortenamt, und CHemische Industrie) phenology were measured. Soil moisture was measured using a Delta-T ML3 Theta-Probe. The soil moisture sensor has three 6 cm rods, resulting in an integrated measuring depth of 0–6 cm. At each sampling site, seven measurements were taken, and their average value was used as the true value for the site. The geolocation of each sampling site was identified using a global positioning system . Soil and crop measurements were randomly taken within a 10 m by 10 m area of each georeferenced site. PAI and vegetation cover fraction were also measured at each sampling site using a Nikon D300S camera equipped with a 10.5 mm fisheye lens [35]. In this study, as RVI was adopted to parameterize vegetation attenuation, only the *in situ* measured soil moisture was used for model calibration and verification, and the BBCH was used to characterize the phenological stages of the soybean field. Details of field measured soil moisture and BBCH are shown in Table I.

B. Synthetic Aperture Radar Data and Preprocessing

RADARSAT-2 was a commercial remote sensing satellite launched on December 14, 2007 by the Canadian Space Agency. It is equipped with a high-resolution C-band (approximately 5.6 cm wavelength) SAR sensor capable of multiple configurations and polarizations. In this study, a total of seven Single Look Complex (SLC) RADARSAT-2 fine-quad polarization (FQP) images covering the three soybean fields acquired from July to October 2015 were used. The FQP has a spatial coverage of 30 $\times$50 km and incidence angles range from 19.5° to 42.3° (see Table II). The nominal spatial resolution of these images was approximately 8 m.

Preprocessing of the RADARSAT-2 data in this study using PolSARpro6.0 [22] includes three steps. First, the T3 matrix was extracted from the original SLC images of RADARSAT-2 acquisitions. Then, in order to reduce the speckle noise, a boxcar filter with 7$\times$7 window size was applied. Finally, the geocoding process was applied to make the T3 matrix corresponding to the radar ground range. The SAR local incidence angle was also obtained for the SAR signal radiometric correction.

III. POLARIMETRIC DECOMPOSITION

The H/α decomposition was introduced first, which is used in this study to help understand the scattering mechanism in soybean fields. Then, the Freeman–Durden three-component polarimetric decomposition was introduced. Based on that, the model-based decomposition method used in this study was presented.

A. H/α Decomposition

The H/α decomposition proposed by Cloude and Pottier [36] provides a means to understand the scattering mechanisms based on eigenanalysis of the covariance or the coherence matrix. Two

TABLE II
COLLECTED SAR DATA

Acquired Date	Day of Year (DOY)	Orbit	Beam	Local Incidence Angle (S09)	Local Incidence Angle (S20)	Local Incidence Angle (S114)
2015.07.17	198	Ascending	FQ10	28.3~33.1	28.3~31.5	28.3~34.6
2015.08.10	222	Ascending	FQ10	28.1~33.1	28.3~32.4	28.3~34.4
2015.09.03	246	Ascending	FQ10	28.5~33.1	28.4~32.2	28.3~34.5
2015.09.13	256	Ascending	FQ20	38.0~43.0	38.2~42.3	38.6~44.2
2015.09.17	260	Ascending	FQ1	18.0~21.5	17.8~21.5	17.0~23.5
2015.09.27	270	Ascending	FQ10	27.8~33.1	28.3~32.4	28.3~34.3
2015.10.01	274	Descending	FQ09	27.4~32.3	27.4~31.1	27.9~33.5

parameters are used to characterize the scattering mechanism, namely, entropy *H,* and polarization angle α, which are derived from the eigenvalues and eigenvectors of the coherency matrix

$$\begin{aligned} H &= \sum_{i=1}^{3} -p_i \log_3 p_i \\ \alpha &= \sum_{i=1}^{3} p_3 \mathrm{a}\cos(|e_{i1}|) \\ p_i &= \frac{\lambda_i}{\sum_{i=1}^{3} \lambda_i} \\ e_i &= [e_{i1} e_{i2} e_{i3}]^T \end{aligned} \tag{1}$$

where H is the entropy, α is the polarization angle, λ_{i} (i = 1, 2, 3) is the eigenvalue of the coherency matrix, while $\mathrm{e_i}$ (i = 1, 2, 3)is the corresponding eigenvector. The H/α decomposition was used to help interpret the scattering mechanism of the soybean fields on different dates.

B. Freeman–Durden Three-Component Decomposition

The Freeman–Durden three-component decomposition decomposed the measured coherency matrix [T3] into surface scattering component (modeled by Bragg), dihedral reflection component (modeled by Fresnel), and volume scattering components with randomly oriented dipole scattering elements

$$\begin{aligned} T3 &= \begin{bmatrix} T_{11} & T_{12} & 0 \\ T_{12}{}^* & T_{22} & 0 \\ 0 & 0 & T_{33} \end{bmatrix} = \mathrm{Ts} + \mathrm{Td} + \mathrm{Tv} \\ &= f_s \begin{bmatrix} 1 & \beta^* & 0 \\ \beta & |\beta|^2 & 0 \\ 0 & 0 & 0 \end{bmatrix} + f_d \begin{bmatrix} |\alpha|^2 & \alpha & 0 \\ \alpha^* & 1 & 0 \\ 0 & 0 & 0 \end{bmatrix} + \frac{f_v}{4} \begin{bmatrix} 2 & 0 & 0 \\ 0 & 1 & 0 \\ 0 & 0 & 1 \end{bmatrix} \end{aligned} \tag{2}$$

where T3 is the coherency matrix measured by the SAR sensor, which is assumed to satisfy the reflection symmetry. Ts, Td, Tv represent the surface, dihedral, and volume scattering component coherency matrix, respectively, β denotes the normalized difference of the Bragg scattering in H and V polarization, α is the normalized difference of the combined ground-stalk Fresnel reflection in H and V polarizations, the *fs*, *fd*, and *fv* are the intensity coefficients of these three scattering components, and the superscript '$*$' denotes the complex conjugate.

The scattering power of surface component ($\mathrm{P_s}$), dihedral component ($\mathrm{P_d}$), and volume component ($\mathrm{P_v}$) are given by the following:

$$\begin{aligned} P_s &= f_s(1 + |\beta|^2) \\ P_d &= f_d(1 + |\alpha|^2) \\ P_v &= f_v. \end{aligned} \tag{3}$$

C. Model-Based Polarimetric Decomposition Used in This Study

An improved model-based decomposition for coherency matrix is adopted in this study, which is based on the Freeman–Durden decomposition. Three main improvements applied on the Freeman–Durden polarimetric decomposition were included in this decomposition method and will be introduced.

The first improvement is adding the deorientation process since each PolSAR pixel may have different orientation angles [32]. This process was applied to our research area since about a quarter of land has a gentle slope. The fluctuation of randomly distributed orientation angles can introduce uncertainty in polarimetric decomposition, leading to a decreased accuracy of the soil moisture retrieval. Thus, the deorientation method proposed by An *et al*. [32] was applied to the PolSAR data before polarimetric decomposition. In the deorientation process, the measured coherency matrix T3 is rotated around the Line of Sight with an angle ϕ as follows:

$$\begin{aligned} \mathrm{T3}(\phi) = &\begin{bmatrix} 1 & 0 & 0 \\ 0 & \cos(2\phi) & \sin(2\phi) \\ 0 & -\sin(2\phi) & \cos(2\phi) \end{bmatrix} \cdot \mathrm{T3} \\ &\cdot \begin{bmatrix} 1 & 0 & 0 \\ 0 & \cos(2\phi) & -\sin(2\phi) \\ 0 & \sin(2\phi) & \cos(2\phi) \end{bmatrix} \end{aligned} \tag{4}$$

ϕ ranges from $-\pi/4$ to $\pi/4$ and is determined through the following equations:

$$\begin{aligned} \cos(4\phi) &= \frac{B}{\sqrt{B^2 + E^2}} \\ \sin(4\phi) &= \frac{E}{\sqrt{B^2 + E^2}}. \end{aligned} \tag{5}$$

B and *E* are derived from the original T3 matrix through the following equations:

$$B = (\mathrm{T}_{22} - \mathrm{T}_{33})/2$$
$$E = \Re(\mathrm{T}_{23}) \tag{6}$$

where T_{ij} denotes the *i*th row and *j*th column element of the original measured T3 matrix; the sign $\Re$ denotes the real part of the complex number.

After the deorientation process, the cross-polarization scattering power is minimized and the copolarization scattering power increases.

The second improvement is the determination of the volume scattering intensity *fv* through the nonnegative eigenvalue decomposition (NNED) method proposed by Van Zyl *et al*. [37] rather than solving the linear equation (2). According to this method, *fv* takes the minimum value that makes the minimum eigenvalue of remaining coherency matrix (i.e., T3–Tv) zero. Three solutions were obtained from (2) shown as follows, and the minimum of them was selected:

$$f_{v1} = \frac{(\mathrm{T}_{11}\mathrm{V}_{22} - 2\Re(T_{12})\mathrm{V}_{12} + \mathrm{T}_{22}\mathrm{V}_{11} + \sqrt{\mathrm{AT}}}{2(V_{11}V_{22} - {V_{12}}^2)}$$
$$f_{v2} = \frac{(\mathrm{T}_{11}\mathrm{V}_{22} - 2\Re(T_{12})\mathrm{V}_{12} + \mathrm{T}_{22}\mathrm{V}_{11} - \sqrt{\mathrm{AT}}}{2(V_{11}V_{22} - {V_{12}}^2)}$$
$$f_{v3} = \frac{\mathrm{T}_{33}}{V_{33}}$$
$$\begin{aligned}\mathrm{AT} = {} & {\mathrm{T}_{11}}^2{\mathrm{V}_{22}}^2 - 4\mathrm{T}_{11}\Re(T_{12})\mathrm{V}_{12}\mathrm{V}_{22} - 2\mathrm{T}_{11}\mathrm{T}_{22}\mathrm{V}_{11}\mathrm{V}_{22} \\ & + 4\mathrm{T}_{11}\mathrm{T}_{22}{\mathrm{V}_{12}}^2 + 4\Im(T_{12})^2\mathrm{V}_{11}\mathrm{V}_{22} - 4\Im(T_{12})^2{\mathrm{V}_{12}}^2 \\ & + 4\Re(T_{12})^2\mathrm{V}_{11}\mathrm{V}_{22} - 4\Re(T_{12})\mathrm{T}_{22}\mathrm{V}_{11}\mathrm{V}_{12} + {\mathrm{T}_{22}}^2{\mathrm{V}_{11}}^2 \\ f_v = {} & \min(f_{v1}, f_{v2}, f_{v3})\end{aligned} \tag{7}$$

where T_{ij} denotes the *i*th row and *j*th column element of the measured T3 matrix; V_{ij} denotes the *i*th row and *j*th column element of the volume scattering coherency matrix; the sign $\Re$ and $\Im$ denote the real and imaginary part of the complex number, respectively.

The third improvement is to ignore the dihedral scattering component in the polarimetric decomposition. The rationality of this modification has been justified in [24], and ignoring the dihedral component could greatly reduce the complexity of soil moisture retrieval from the remaining scattering component. Thus, the coherency matrix of the agricultural field can be expressed as follows:

$$\mathrm{T3} = \mathrm{Ts} + \mathrm{Tv} = \mathrm{Ts} + \frac{f_v}{4} \cdot \begin{bmatrix} 2 & 0 & 0 \\ 0 & 1 & 0 \\ 0 & 0 & 1 \end{bmatrix}. \tag{8}$$

After applying the improved model-based decomposition on RADARSAT-2 data, the coherency matrix corresponding to surface scattering component could be obtained and the attenuated surface backscattering coefficients could be derived using the following equation:

$$\sigma^o_{HH\_\mathrm{surface}} = (Ts_{11} + Ts_{12} + {Ts_{12}}^* + Ts_{22})/2$$
$$\sigma^o_{VV\_\mathrm{surface}} = (Ts_{11} - Ts_{12} - {Ts_{12}}^* + Ts_{22})/2 \tag{9}$$

where Ts_{ij} denotes the *i*th row and *j*th column element of the Ts matrix, $\sigma^{\mathrm{o}}_{HH\_\mathrm{surface}}$, $\sigma^{\mathrm{o}}_{HV\_\mathrm{surface}}$, $\sigma^{\mathrm{o}}_{VV\_\mathrm{surface}}$ denote the surface backscattering coefficients in power after the removal of volume scattering effect.

SAR local incidence angle generally has a significant impact on the observed backscattering coefficient, which cannot be ignored in soil moisture retrieval. To constrain the effect of the different local incidence angles, a theoretical approach proposed by Ulaby *et al*. [38] was adopted to reduce the effect of local incidence angle after decomposition

$$\sigma^o_{\theta_{\mathrm{ref}}} = \sigma^o_\theta \frac{\cos^2\theta_{\mathrm{ref}}}{\cos^2\theta} \tag{10}$$

where θ_{ref} represents the reference incidence angle, and θ is the local incidence angle. According to the incidence angle range of time-series RADARSAT-2 images and the application range of the Dubois model [14], [39], the reference incidence angle θ_{ref} was set to 40° in this study.

IV. Soil Moisture Retrieval After Decomposition

A. Soil Surface Backscattering Modeling

The Dubois model was employed in this study to determine the backscattering of the underlying soil of agricultural fields for mainly two reasons. First, the modeling results under the condition that $\mathrm{m_v} < 35$ vol.%, $k{\cdot}s < 2.5$, and $\theta > 30°$ [14], [39] greatly fit the agricultural field condition in this study. Second, the relationship between soil dielectric constant and backscatter coefficient is reversible, through which soil moisture can be obtained directly without any look-up table construction. The Dubois model expresses the backscatter coefficient as a function of surface parameters (RMS height, soil dielectric constant) and radar sensor parameters (polarization, incidence angle, and wavelength) shown as follows:

$$\sigma^o_{hh} = 10^{-2.75}\frac{\cos^{1.5}\theta}{\sin^5\theta}10^{0.028\varepsilon\tan\theta}(ks\times\sin\theta)^{1.4}\lambda^{0.7}$$
$$\sigma^o_{vv} = 10^{-2.35}\frac{\cos^3\theta}{\sin^3\theta}10^{0.046\varepsilon\tan\theta}(ks\times\sin\theta)^{1.1}\lambda^{0.7} \tag{11}$$

where ε is the soil dielectric constant, which can be transformed to soil moisture through a dielectric constant model [33], [34]; *s* is the root mean square (RMS) height of the surface roughness in cm; *k* is free space wave number given by $\mathrm{k} = 2\pi/\lambda$; λ is the wavelength in centimeter; and θ is the incidence angle.

B. Vegetation Attenuation Effect Compensating

Due to limited penetration depth of the C-band SAR, vegetation attenuation is significant and should not be ignored in soil moisture estimation. The two-way attenuation parameter of the surface vegetation layer in WCM [26] was adopted to describe the vegetation attenuation effect:

$$\tau^2 = e^{-2b\cdot V/\cos\theta} \tag{12}$$

where τ^2 is the two-way attenuation parameter; *b* is an empirical coefficient requiring calibration using *in situ* measurements; V is the vegetation canopy description that is parameterized by vegetation index such as VWC, LAI, and Normalized Difference

Vegetation Index, etc. As microwave signal is sensitive to water content, VWC is usually selected to parameterize the signal; however, the VWC usually relies on *in situ* measurement or optical remote sensing. Kim *et al*. found a strong relationship between RVI and VWC, demonstrating that RVI is a robust method for characterizing vegetation canopy [40]. Thus, RVI was used to parameterize the two-way attenuation in this study. The RVI is given by the following:

$$RVI = \frac{8\sigma^o_{HV}}{\sigma^o_{HH} + \sigma^o_{VV} + 2\sigma^o_{HV}} \tag{13}$$

where $\sigma^{\rm o}_{HV}$ is the cross-polarization backscatter coefficient in power; and $\sigma^{\rm o}_{HH}$, $\sigma^{\rm o}_{VV}$ are the co-polarization backscatter coefficients.

Through the two-way attenuation parameter, the relationships between surface backscatter coefficients after polarimetric decomposition and the Dubois modeled backscatter coefficients are established

$$\begin{aligned}\sigma^o_{HH\_\rm surface} &= \tau^2 \cdot \sigma^o_{HH\_\rm dubois} = e^{-2b\cdot RVI/\cos\theta} \cdot \sigma^o_{HH\_\rm dubois} \\ \sigma^o_{VV\_\rm surface} &= \tau^2 \cdot \sigma^o_{VV\_\rm dubois} = e^{-2b\cdot RVI/\cos\theta} \cdot \sigma^o_{VV\_\rm dubois}.\end{aligned} \tag{14}$$

Furthermore, by substituting (11) into (14) and inverting the equation, the relationships between backscattering coefficients and soil dielectric constant can be expressed as follows:

$$\begin{aligned}\varepsilon(HH) &= \log_{10}\left[\frac{\sigma^o_{HH}\cdot\sin^3\theta}{10^{-2.75}\cdot e^{-2b\cdot RVI/\cos\theta}\cdot\lambda^{0.7}\cdot\cos^{1.5}\theta\cdot(ks\cdot\sin\theta)^{1.4}}\right]\Big/ 0.028\tan\theta \\ \varepsilon(VV) &= \log_{10}\left[\frac{\sigma^o_{VV}\cdot\sin^3\theta}{10^{-2.35}\cdot e^{-2b\cdot RVI/\cos\theta}\cdot\lambda^{0.7}\cdot\cos^{3}\theta\cdot(ks\cdot\sin\theta)^{1.1}}\right]\Big/ 0.046\tan\theta.\end{aligned} \tag{15}$$

Soil moisture *Mv* can be calculated through Topp's dielectric mixing model [33]

$$\begin{aligned}Mv = &-5.3\times10^{-2} + 2.92\times10^{-2}\varepsilon - 5.5 \\ &\times10^{-4}\varepsilon^2 + 4.3\times10^{-6}\varepsilon^3.\end{aligned} \tag{16}$$

For convenience, the established relationship is referred as the coupled model, through which the soil moisture can be directly obtained by surface backscatter coefficients after polarimetric decomposition.

C. Optimum Surface Roughness Parameter

Apart from vegetation cover effect, soil moisture retrieval is also largely influenced by surface roughness parameters. However, precise measurement of surface roughness is very difficult due to the measurement technique and dense vegetation cover [16]. Therefore, optimum surface roughness proposed by Bai *et al*. [9] was used to parameterize the Dubois surface scattering model.

The procedure for determining the optimal roughness parameter is a process of selecting the optimal roughness value in a predefined range. In this study, the predefined range of optimal roughness (i.e., RMS height *s*) is set from 1 to 30 mm with $\triangle s =$ 1 mm, suitable for typical roughness condition over agricultural fields [41].

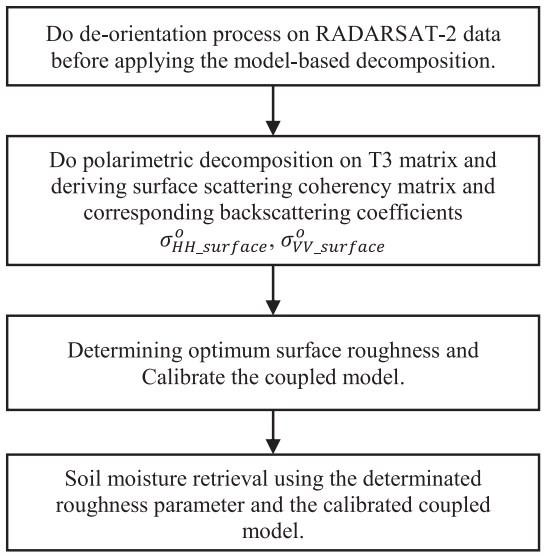

Fig. 3. Schematization of the proposed soil moisture retrieval method.

D. Process of the Soil Moisture Retrieval Algorithm

The soil moisture retrieval algorithm proposed in this study includes the following four major steps as illustrated in Fig. 3.

1) Perform the deorientation process on RADARSAT-2 data before the model-based decomposition. Then the measured coherency matrix T3 without the effect of orientation angle could be derived.
2) Perform polarimetric decomposition on measured T3 matrix after deorientation, including the determination of volume scattering intensity and deriving surface scattering coherency matrix. Surface scattering backscattering coefficients are subsequently obtained.
3) Determining optimum surface roughness and calibrating the coupled model (details are shown in Fig. 4). First, the decomposed surface backscatter coefficients $\sigma^{\rm o}_{HH\_\rm surface}$, $\sigma^{\rm o}_{VV\_\rm surface}$, measured soil moisture, RVI and the RMS height *s* in the predefined range (i.e., $s = 1$ to 30 mm) are used to calibrate the coupled model through the least-squares fitting method. Retrieved soil moisture are subsequently obtained and RMSE is calculated using *in situ* soil moisture measurements. Then update the RMS height *s* in the predefined range until *s* reaches up to 30 mm. The value of RMS height *s* corresponding to minimum RMSE is selected as the optimal surface roughness. Then, calibrate the coupled model using the optimal surface roughness.
4) Retrieve soil moisture using the determined optimal roughness parameter and the established coupled model. After that, the result is validated using the *in situ* measurements.

V. Result and Discussion

A. Scattering Mechanisms Analysis

The H/α decomposition introduced in Section III-A was used to help understand the scattering mechanisms in the soybean fields, and the H/α plane on different dates are shown in Fig. 5.

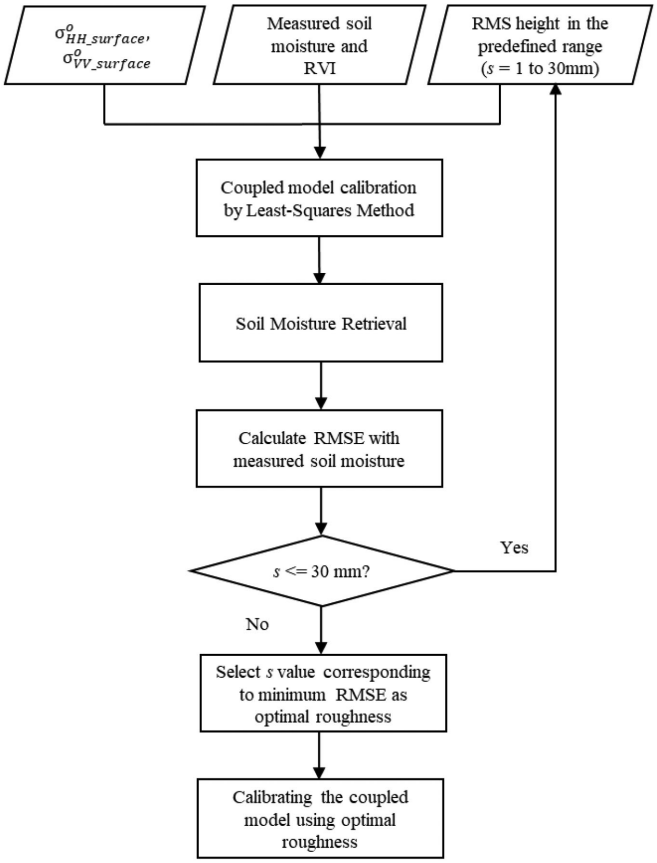

Fig. 4. Schematization of optimum surface roughness determination and the coupled model calibration.

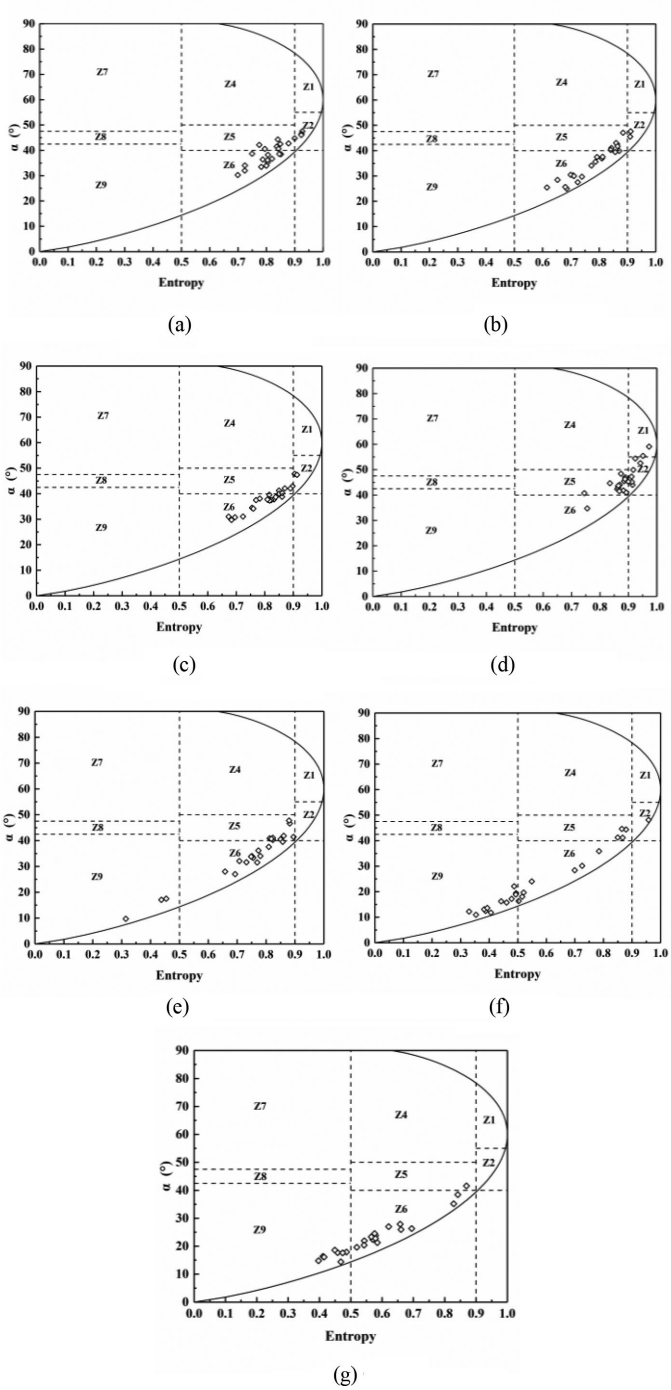

Fig. 5. H and α plots over soybean fields in different date. (a) July 17, (b) August 10. (c) September 03. (d) September 13. (e) September 17. (f) September 27. (g) October 01.

From July 17 to September 13, the scatters in the H/α plane were relatively dense, mainly distributed in Z6, Z5, and Z2. This suggests that the dominant volume scattering or dominant surface scattering with the effect of vegetation attenuation. From September 17 to October 1, the scatters in the H/α plane became more dispersed. More scatters are located in Z9 with a lower value of H and α, showing dominant surface scattering.

According to ground data, soybean was sown in May and its canopy was relatively dense in July. From July 17 to September 13, the soybean canopy was well developed with relative high vegetation coverage. Since September 17, the vegetation cover value decreased rapidly, indicating the coming of late growth stage. The temporal evolution of H/α agreed well with its growth.

Meanwhile, it is noted that the scatters on the H/α plane for September 13 were less located in Z6 compared with July 17, August 10, and September 3. This is due to the relatively high incidence angle (around 40°) of the RADARSAT-2 image on this date compared with the SAR data on other acquisition dates (around 20° or 30°) as the surface scattering component is more significant at low incidence angle [11].

In addition to the H/α decomposition, the Freeman–Durden three-component polarimetric decomposition with the first and second improvement in Section III-C (i.e., deorientation process and determine fv by NNED) was used to further explain the scattering mechanisms. Fig. 6 illustrates the percentage of the surface, dihedral and volume scattering power on different dates in these three soybean fields. The scattering power of volume scattering from July 17 to September 3 was higher than September 17 to October 1, while the percentage of surface component scattering power shows a reversed tendency. This phenomenon is consistent with the temporal evolution of H/α as well as the vegetation phenology change. Meanwhile, it is observed that the surface scattering power on September 13 was obviously lower

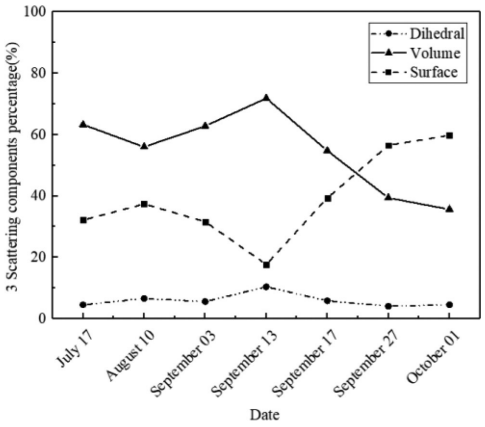

Fig. 6. Time-series distribution of dihedral, volume, and surface scattering power in percentage.

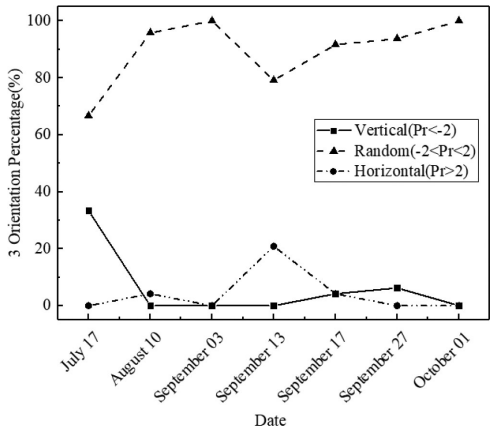

Fig. 7. Time-series distribution of vertical, random, and horizontal vegetation orientation percentage.

than July 17 to September 3, agreeing with the result by H/α decomposition.

Besides, it is worth noting that over the entire soybean growing period, the dihedral scattering component only accounted for a small fraction (3.1% to 9.9%) of the total scattering power. Therefore, it is reasonable to ignore the dihedral scattering component in the polarimetric decomposition to greatly simplify the procedure of soil moisture retrieval through the remaining components.

B. Vegetation Orientation Analysis

The copolarization power ratio *Pr* proposed in [42] was used to analyze the orientation of dipoles in soybean fields, which is defined as follows:

$$P_r = 10 \cdot \log \frac{< |S_{VV}|^2 >}{< |S_{HH}|^2 >}. \tag{17}$$

If *Pr* is less than –2 dB, vertically oriented dipoles are assumed; if *Pr* is between –2 and 2 dB, randomly oriented dipoles are assumed; for *Pr* that is higher than 2 dB, horizontally oriented dipoles are assumed.

The percentages of vertical, random, and horizontal vegetation orientation points at different growth stages are illustrated in Fig. 7. Throughout the entire soybean growing period, although the phenology and crop structure vary with vegetation growth, random orientation is dominant, accounting for a fraction of 67% to 100%. Overall, the sample sites with random orientation vegetation take up to 81.3% of the total sample sites of all dates. This result is consistent with the conclusions reported by Moran *et al*. that soybean is mainly characterized by random scatters [43]. Thus, unlike selecting the adaptive volume coherency matrix dynamic [24], [31], we only used the random scattering coherency matrix to describe volume scattering due to random orientation accounts for the vast majority in total.

C. Sensitivity of Soil Moisture to RMS Height

As mentioned in Section IV-C, soil moisture retrieval over vegetation areas also greatly influenced by surface roughness. Fig. 8 illustrates the relationship between the retrieved soil moisture and SAR backscatter coefficients through the Dubois model and Topp's dielectric mixing model with different RMS height *s*. RMS height was set from 0.5 to 1.4 cm, with a step size of 0.3 cm (corresponding to different curves in Fig. 8). Other parameters were set to constants according to RADARSAT-2 configuration and field situation as follows: incidence angle: 40°, wavelength: 5.5504 cm, wavenumber: 1.132 rad/cm.

As illustrated in Fig. 8, the sensitivity of backscatter coefficients to soil moisture increases as soil moisture increases. When soil moisture is high ($Mv > 40$ vol.%, even sometimes $Mv >$ 0.35 vol.%), the sensitivity of backscattering coefficients to soil moisture is extremely high which makes it difficult to estimate soil moisture through the coupled model. For dry soil ($Mv <$ 10 vol.%), the backscattering coefficients are less sensitive to soil moisture changes. Thus, a small variation in backscatter coefficients will lead to a significant change in the estimated soil moisture, introducing more uncertainties in the retrieved soil moisture.

Besides, the RMS height has a great impact on the soil moisture (illustrated by the different curves in Fig. 8). As the RMS height increases, smaller soil moisture would be derived for a certain backscatter coefficient. Furthermore, the sensitivity of the backscattering coefficients to soil moisture also varies with RMS height. As the backscatter coefficients increase, the radar backscatter signal will saturate quickly with a higher RMS height value. A small change in RMS height can lead to a significant difference in the retrieved soil moisture for a certain backscattering coefficient. Therefore, optimum surface roughness proposed by Bai *et al*. [9] was used to the Dubois model for subsequent soil moisture retrieval.

D. Validation of Underlying Backscattering Modeling and Deorientation Process

To evaluate the Dubois model for describing the underlying soil backscattering, modeled backscatter coefficients were derived using the coupled model with measured soil moistures as inputs. Fig. 9 shows the scatterplots between the modeled

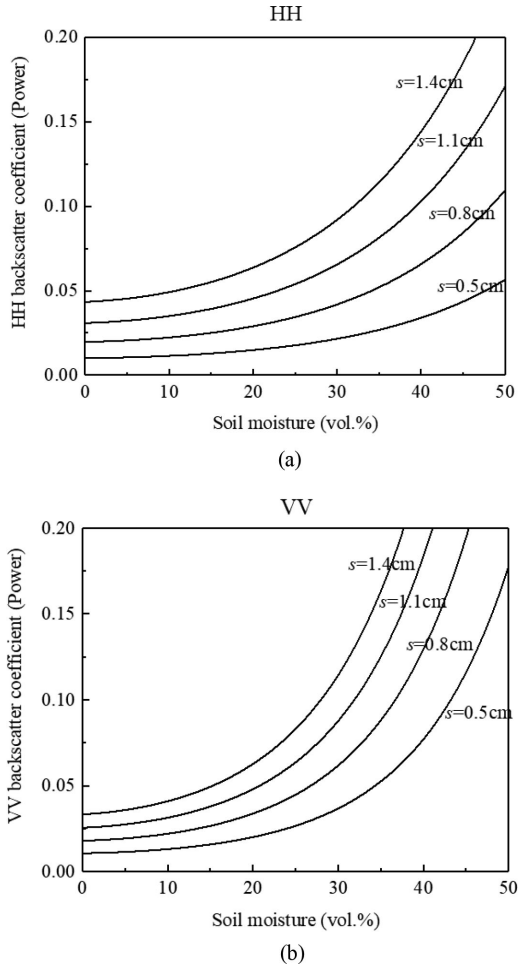

Fig. 8. Relationship between soil moisture and backscatter coefficients at different RMS height at (a) HH polarization and (b) VV polarization.

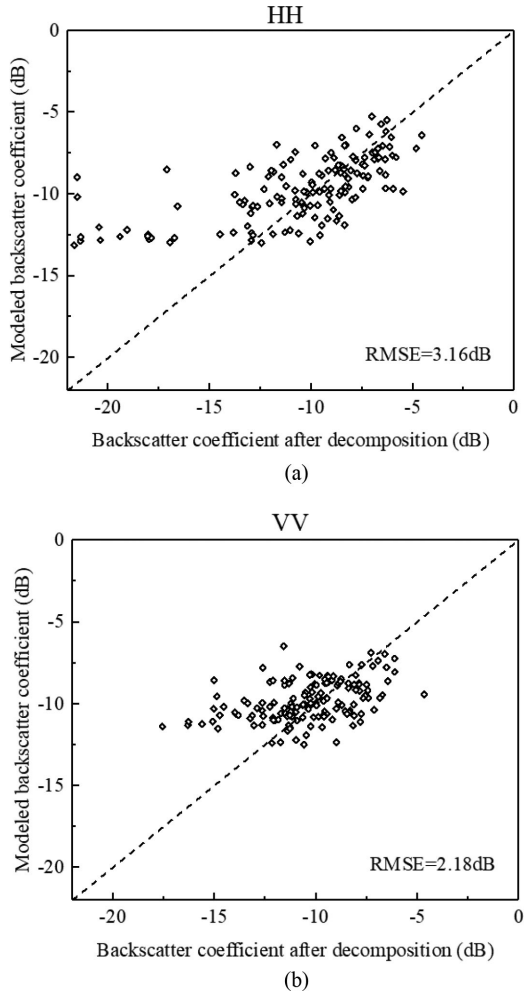

Fig. 9. Scatterplots between modeled backscatter coefficients and backscatter coefficient after polarimetric decomposition at (a) HH polarization and (b) VV polarization.

backscatter coefficients and backscatter coefficients after polarimetric decomposition. The RMSE between the modeled and decomposed backscatter coefficients were 3.16 and 2.18 dB at HH and VV polarization, respectively, indicating a better performance of the coupled model in VV polarization. It is found in Fig. 8(a) that several points have a bigger bias between the modeled and decomposed HH backscatter coefficients. This phenomenon could have been attributed to the extremely small value of the decomposed backscatter coefficients at these points, exceeding the validity range of the Dubois model. Overall, the discrepancy between the modeled and decomposed backscatter coefficients is acceptable with relatively low RMSE value.

E. Deorientation Process and the Choice of Reference Incidence Angle

Fig. 10 illustrates the histogram of the orientation angles for all seven SAR images. The random distribution of orientation angles is obvious, consistent with the topography in our study that about a quarter of fields have a gentle slope, and it also confirms with the requirement of the deorientation process. The soil moisture retrieval results before and after applying the deorientation process on T3 matrix are shown in Table III. Correlation coefficient R and RMSE were used to evaluate the accuracy of the retrieved soil moisture. As shown in Table III, the accuracy of the retrieved soil moisture is improved for both HH and VV polarization after applying the deorientation process. This can be attributed to the more accurate polarimetric decomposition result using $\mathrm{T3}(\phi)$. The deorientation process of the measured coherency matrix T3 can minimize the cross-polarized scattering power and increase the copolarized scattering power. The rotated $\mathrm{T3}(\phi)$ is assumed to satisfy the reflection symmetry better, which is a premise of the model-based polarimetric

TABLE III
SOIL MOISTURE RETRIEVAL RESULT BEFORE AND AFTER APPLYING DEORIENTATION

	HH		VV	
	R	RMSE	R	RMSE
Before Applying Deorientation	0.62	9.7vol.%	0.60	9.3vol.%
After Applying Deorientation	0.64	9.2vol.%	0.68	8.2vol.%

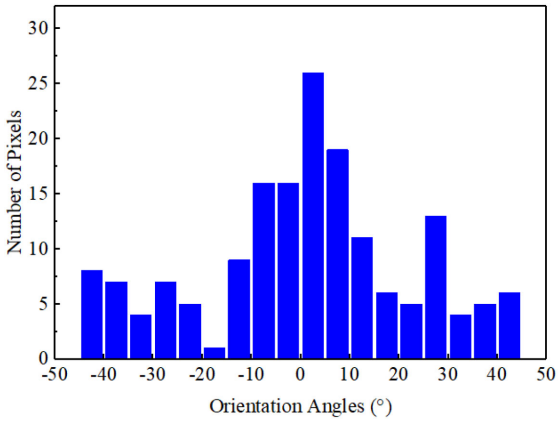

Fig. 10. Histogram of the orientation angles for all seven SAR images.

TABLE IV
RMSE OF BETWEEN RETRIEVED AND MEASURED SOIL MOISTURE

Reference Incidence Angle	HH	VV
30°	12.0vol.%	10.3vol.%
35°	10.5vol.%	8.9 vol.%
40°	9.2vol.%	8.2vol.%

decomposition. Thus, the introduction of deorientation process does benefit soil moisture retrieval through polarimetric decomposition.

As reported in [44], apart from volumetric scattering, there are three possible reasons for the presence of cross polarization:

1) presence of oblique dihedral;
2) presence of azimuth terrain slope; and
3) presence of soil surface roughness.

The first one is not of interest in agricultural applications. The second one is relieved by the deorientation process. The third one is neglected in our study. Although this might bring some uncertainties, we assume the neglection is acceptable since the soybean fields in our study site usually go through seedbed preparation before sowing; hence, the field is rather smooth.

The choice of the reference angle related to the used surface backscattering model. Considering the validity incidence angle range of the Dubois model ($\theta > 30°$) and our dataset. Soil moisture was retrieved under three incidence angles (30°, 35°, and 40°). The RMSE of the retrieval result at different angle in HH and VV polarization was illustrated in Table IV. From Table IV, it is observed that the soil moisture retrieval method performed better at a higher reference incidence angle. This is consistence with Dubois model's validity range. At HH polarization, the better modeling result when $\theta \geq 34°$ also explained this phenomenon [45]. Thus, the reference incidence angle was chosen to be 40°.

F. Retrieved Soil Moisture

In order to evaluate the performance of the proposed method for soil moisture retrieval under vegetation cover, the leave-one-out-cross-validation (LOOCV) method was adopted. For the sample sites corresponding to a specific date, only one of the data samples was used as the validation set and the remaining n-1 data samples were used as the training set. This is repeated in all ways until all sample sites have been used as the validation set once. The result of this LOOCV evaluation is generally regarded as a more conservative estimate of the model performance than that trained on all samples [46]. Over a very few sample sites, typically where *in situ* measured soil moisture near zero, the retrieved soil moisture is negative. However, soil moisture is always a nonnegative value according to its physical implication. Thus, these negative values were set to zero.

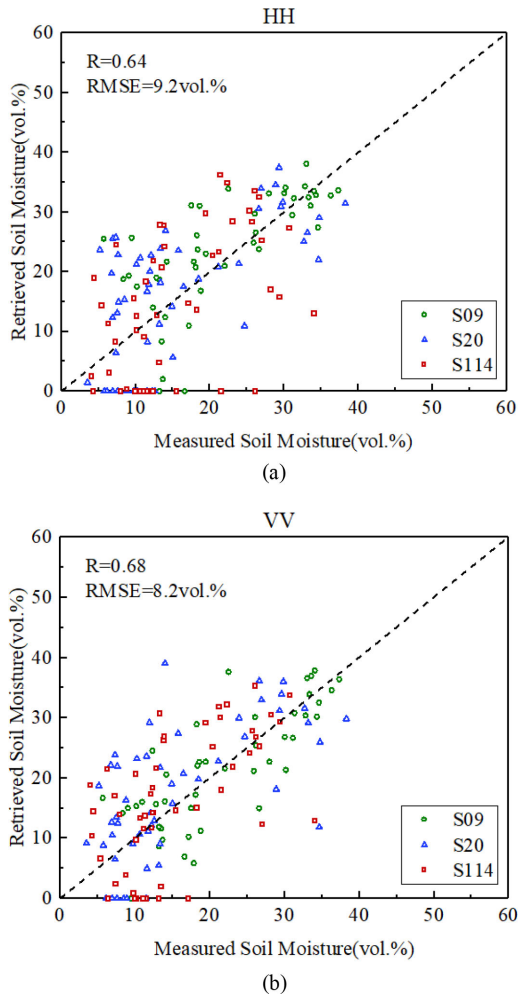

Fig. 11. Scatterplots between measured and retrieved soil moisture through (a) HH polarization and (b) VV polarization.

The retrieved soil moistures with their respective measured soil moistures of three soybean fields (S09, S20, S114) are illustrated in Fig. 11. The retrieval results using HH and VV polarization are shown in Fig. 11(a) and (b), respectively. The linear relationship between the estimated and measured soil moisture was observed with a correlation coefficient R of 0.68 and an RMSE of 8.2 vol.% at VV polarization, revealing that the method proposed here is capable of estimating soil moisture for soybean field during the growing season. The accuracy of

TABLE V
RMSE OF BETWEEN RETRIEVED AND MEASURED SOIL MOISTURE

	HH	VV
S09	7.7vol.%	6.2vol.%
S20	9.0vol.%	9.1 vol.%
S114	10.5vol.%	8.9 vol.%
total	9.2vol.%	8.2vol.%

retrieved soil moisture is slightly lower at HH polarization than at VV polarization with a correlation coefficient R of 0.64 and an RMSE of 9.2 vol.%. Better performance of the proposed soil moisture retrieval method at VV polarization than at HH polarization was found, with or without applying the deorientation process on the SAR data. The reason lies in two main aspects. First, better performance of the Dubois model at VV polarization than at HH polarization was found in [45]. Besides, the weaker double-bounce scattering power at VV polarization than HH polarization also contributes to this phenomenon [47].

For dry soil, especially when *in situ* measured soil moisture is below 10 vol.%, several estimated soil moisture values are zero as illustrated in Fig. 11. This is mainly due to the extremely low sensitivity of the SAR backscatter coefficients to soil moisture changes under dry soil conditions (as illustrated in Fig. 8). Thus, the backscatter coefficient is hard to reveal the soil moisture variability under this condition, which brings in more uncertainty in the retrieved soil moisture. Among the three fields, S09 outperformed S20 and S114 (see Table V). Field condition might have contributed to this variation in model performance. The soybean growth in field S09 was more uniform than that in the other two fields.

Fig. 12 depicts the temporal evolution of the retrieved soil moisture and measured soil moisture. Within the data acquisition period from July 2015 to October 2015, the trend of the time-series of measured soil moisture was well reproduced by the estimated soil moisture, especially at VV polarization. However, soil moistures were found to be overestimated at late growth stage when vegetation cover was sparse because the soybean plants had shed their leaves. This might be attributed to the deorientation process before polarimetric decomposition. To our knowledge, the deorientation process applied on T3 matrix can minimize T_{33}, through which the volume scattering was determined. Thus, the polarimetric decomposition might underestimate the volume scattering power while overestimate surface scattering power, leading to an overestimate of retrieved soil moisture at late growth stage. To help understanding the soil moisture variabilities, the retrieved soil moisture images through VV polarization are depicted in Fig. 13.

Fig. 14 illustrates the RMSE between the retrieved and measured soil moistures on different dates. On most dates, the VV polarization has a better performance than HH polarization. During the entire growing season, the RMSE of the retrieved soil moisture at VV polarization varies little. Even during the mid-growth stage when vegetation cover was dense, the

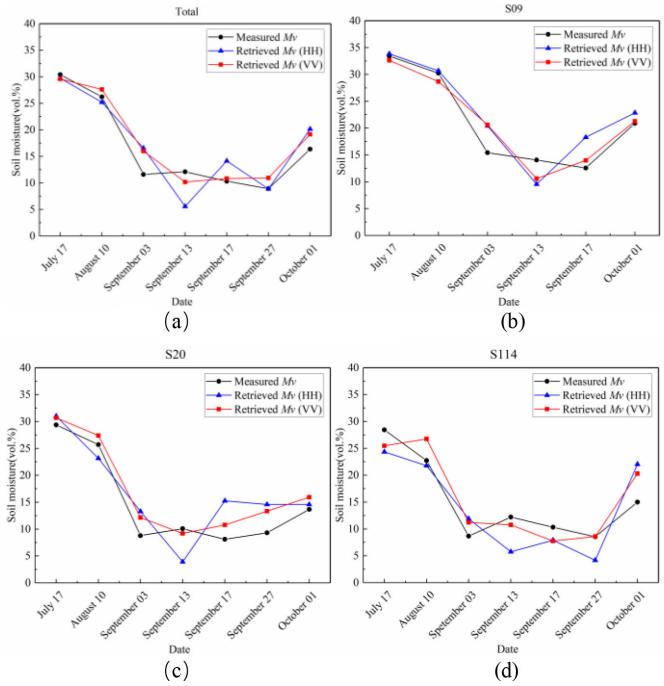

Fig. 12. Temporal evolution of measured and retrieved soil moisture (a) Total. (b) S09. (c) S20. (d) S114.

RMSE of the retrieved soil moisture is still satisfactory. Thus, the proposed method is capable of monitoring soil moisture variation throughout the soybean growing season. However, although vegetation cover is sparser at late growth stage than at mid-growth stages, a better retrieval result was not achieved. This might because soybean plants were senescent and very dry, resulting in an underestimate of volume scattering component and subsequently affects the retrieved soil moisture accuracy.

Our soil moisture retrieval results are comparable with the results achieved by Wang [24] (RMSE of retrieved soil moisture is no more than 7.4 vol.%), which used the Oh model to describe surface scattering under vegetation cover and VWC to parameterize the vegetation attenuation. In our study, RVI and optimal surface roughness were adopted to parameterize the vegetation two-way attenuation and Dubois model, respectively, without having to rely on prior vegetation indices and roughness parameter.

In this study, the RMSE of soil moisture estimation came mainly from the following.

1) Underlying soil backscattering modeling: the Dubois model is inherently a semi-empirical model that needs calibration before applying it to new study sites.
2) Optimal surface roughness: the complex field situation in which the surface roughness condition is not uniform can limit the accurate estimation of soil moisture.
3) The calibration process of the coupled model: the least-squares fitting method may capture the local minima which does not correspond to the global optimum [48].
4) Parameterizing two-way attenuation index through RVI: this might have been affected by the extremely low moisture content of the soybean plants once senesced at late

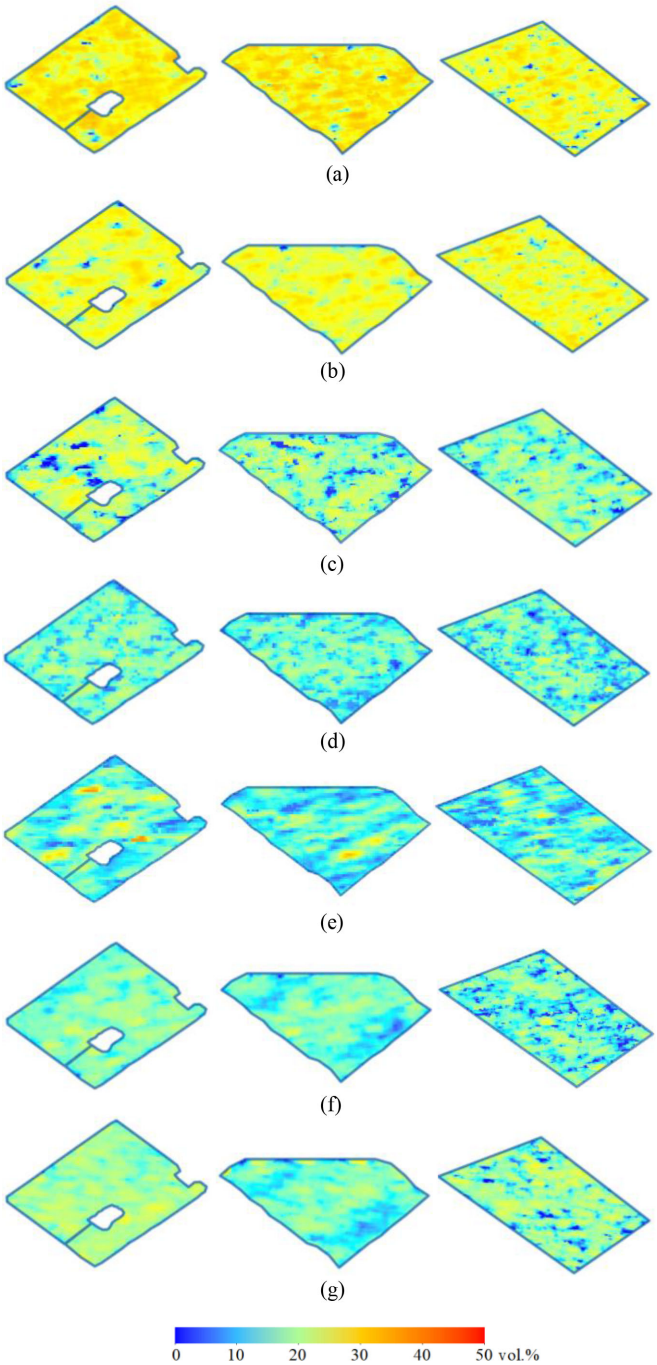

Fig. 13. Soil moisture in S09 (left column), S20 (middle column), and S114 (right column) on different dates (a) July 17. (b) August 10. (c) September 3. (d) September 13. (e) September 17. (f) September 27. (g) October 1.

growth stage. These issues need to be further investigated in future studies.

5) The negligence of soil roughness effect in decomposition: this might lead to an overestimation of volume scattering component and could be solved by using more refined models (X-Bragg, polarimetric two-scale model (PTSM) [49], etc.).

Given the aforementioned uncertainties in the retrieved soil moisture, however, these sources of error are minor. The soil

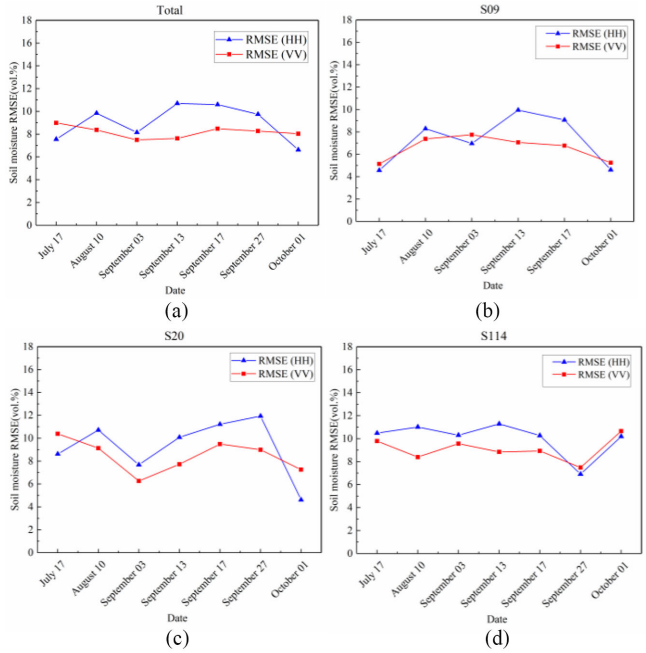

Fig. 14. RMSE and bias between the retrieved and measured soil moisture in different vegetation phenology.

moisture retrieval method proposed in this study is capable of estimating soil moisture over soybean fields during growing season. The main benefit of the proposed method is that only *in situ* measured soil moisture is required for calibrating the coupled model, which can greatly reduce the dependence on prior roughness parameters and vegetation indices.

VI. Conclusion

This study acknowledged the problem that soil moisture retrieval using SAR in agricultural area is challenged by volume scattering and vegetation attenuation during the growing season. To remove the effect of vegetation volume scattering, a model-based polarimetric decomposition was adopted, and the deorientation process of SAR data was applied before polarimetric decomposition to remove the influence of randomly distributed target orientation angles for improved decomposition accuracy. To compensate the effect of vegetation attenuation, a two-way attenuation parameter in WCM was adopted, which is parameterized by RVI in this study. The Dubois model was adopted to model the underlying soil backscattering. Besides, the optimal surface roughness and Topp's dielectric mixing model were used to parameterize the Dubois model and transfer soil dielectric constant to soil moisture, respectively. Desirable results were achieved with R equal to 0.64 and 0.68, RMSE equal to 9.2 vol.% and 8.2 vol.% at HH and VV polarization, respectively. These results are comparable with the soil moisture retrieval result reported in [24], which combined model-based polarimetric decomposition and Oh model to retrieval soil moisture and achieved an RMSE no more than 7.4 vol.%. Our proposed method can greatly reduce the dependence on prior surface roughness parameters and vegetation indices. Besides, soil

moisture was also retrieved without applying deorientation process with RMSE equal to 9.7 vol.% and 9.3 vol.% at HH and VV polarization, respectively, demonstrating that the introduction of the deorientation process does benefit soil moisture retrieval through polarimetric decomposition. These results demonstrate that the proposed method is capable of estimating soil moisture in soybean fields during the growing season.

ACKNOWLEDGMENT

The authors would like to thank A&L Canada Laboratories Inc., for providing soil texture data, and members of Geographic Information Technology and Application Laboratory at the University of Western Ontario for helping collect surface soil moisture and surface roughness measurements.

REFERENCES

[1] H. Lievens, H. Vernieuwe, J. Alvarez-Mozos, B. De Baets, and N. E. C. Verhoest, "Error in radar-derived soil moisture due to roughness parameterization: An analysis based on synthetical surface profiles," *Sensors*, vol. 9, no. 2, pp. 1067–1093, Feb. 2009.

[2] S. G. Wang, X. Li, X. J. Han, and R. Jin, "Estimation of surface soil moisture and roughness from multi-angular ASAR imagery in the watershed allied telemetry experimental research (WATER)," *Hydrol. Earth System Sci.*, vol. 15, no. 5, pp. 1415–1426, 2011.

[3] R. Prakash, D. Singh, and N. P. Pathak, "A fusion approach to retrieve soil moisture with SAR and optical data," *IEEE J. Sel. Topics Appl. Earth Observ. Remote Sens.*, vol. 5, no. 1, pp. 196–206, Feb. 2012.

[4] E. De Keyser, H. Vernieuwe, H. Lievens, J. Alvarez-Mozos, B. De Baets, and N. E. C. Verhoest, "Assessment of SAR-retrieved soil moisture uncertainty induced by uncertainty on modeled soil surface roughness," *Int. J. Appl. Earth Observ. Geoinf.*, vol. 18, pp. 176–182, Aug. 2012.

[5] Y. S. Bao, Y. J. Zhang, J. Z. Wang, and J. Z. Min, "Surface soil moisture estimation over dense crop using Envisat ASAR and Landsat TM imagery: An approach," *Int. J. Remote Sens.*, vol. 35, no. 16, pp. 6190–6212, 2014.

[6] X. F. Zhang, J. P. Zhao, and J. Tian, "A robust coinversion model for soil moisture retrieval from multisensor data," *IEEE Trans. Geosci. Remote Sens.*, vol. 52, no. 8, pp. 5230–5237, Aug. 2014.

[7] M. Xing *et al.*, "Retrieving surface soil moisture over wheat and soybean fields during growing season using modified water cloud model from Radarsat-2 SAR data," *Remote Sens.*, vol. 11, no. 16, 2019, Art. no. 1956.

[8] B. B. He, M. F. Xing, and X. J. Bai, "A synergistic methodology for soil moisture estimation in an alpine prairie using radar and optical satellite data," *Remote Sens.*, vol. 6, no. 11, pp. 10966–10985, Nov. 2014.

[9] X. J. Bai, B. B. He, and X. W. Li, "Optimum surface roughness to parameterize advanced integral equation model for soil moisture retrieval in prairie area using Radarsat-2 data," *IEEE Trans. Geosci. Remote Sens.*, vol. 54, no. 4, pp. 2437–2449, Apr. 2016.

[10] K. C. Kornelsen and P. Coulibaly, "Advances in soil moisture retrieval from synthetic aperture radar and hydrological applications," *J. Hydrol.*, vol. 476, pp. 460–489, Jan Jul. 2013.

[11] H. Wang, R. Magagi, K. Goita, T. Jagdhuber, and I. Hajnsek, "Evaluation of simplified polarimetric decomposition for soil moisture retrieval over vegetated agricultural fields," *Remote Sens.*, vol. 8, no. 2, 2016, Art. no. 142.

[12] C. F. Ma, X. Li, C. Notarnicola, S. G. Wang, and W. Z. Wang, "Uncertainty quantification of soil moisture estimations based on a Bayesian probabilistic inversion," *IEEE Trans. Geosci. Remote Sens.*, vol. 55, no. 6, pp. 3194–3207, Jun. 2017.

[13] Y. Oh, K. Sarabandi, and F. T. Ulaby, "An empirical-model and an inversion technique for radar scattering from bare soil surfaces," *IEEE Trans. Geosci. Remote Sens.*, vol. 30, no. 2, pp. 370–381, Mar. 1992.

[14] P. C. Dubois, J. Vanzyl, and T. Engman, "Measuring soil-moisture with imaging radars," *IEEE Trans. Geosci. Remote Sens.*, vol. 33, no. 4, pp. 915–926, Jul. 1995.

[15] A. K. Fung, Z. Q. Li, and K. S. Chen, "Backscattering from a randomly rough dielectric surface," *IEEE Trans. Geosci. Remote Sens.*, vol. 30, no. 2, pp. 356–369, Mar. 1992.

[16] R. Bryant *et al.*, "Measuring surface roughness height to parameterize radar backscatter models for retrieval of surface soil moisture," *IEEE Geosci. Remote Sens. Lett.*, vol. 4, no. 1, pp. 137–141, Jan. 2007.

[17] M. Callens, N. E. C. Verhoest, and M. W. J. Davidson, "Parameterization of tillage-induced single-scale soil roughness from 4-m profiles," *IEEE Trans. Geosci. Remote Sens.*, vol. 44, no. 4, pp. 878–888, Apr. 2006.

[18] M. Zribi and M. Dechambre, "A new empirical model to retrieve soil moisture and roughness from C-band radar data," *Remote Sens. Environ.*, vol. 84, no. 1, pp. 42–52, Jan. 2003.

[19] N. Baghdadi, C. King, A. Chanzy, and J. P. Wigneron, "An empirical calibration of the integral equation model based on SAR data, soil moisture and surface roughness measurement over bare soils," *Int. J. Remote Sens.*, vol. 23, no. 20, pp. 4325–4340, Oct. 2002.

[20] Z. Su, P. A. Troch, and F. P. DeTroch, "Remote sensing of bare surface soil moisture using EMAC/ESAR data," *Int. J. Remote Sens.*, vol. 18, no. 10, pp. 2105–2124, 1997.

[21] I. Hajnsek, T. Jagdhuber, H. Schon, and K. P. Papathanassiou, "Potential of estimating soil moisture under vegetation cover by means of PolSAR," *IEEE Trans. Geosci. Remote Sens.*, vol. 47, no. 2, pp. 442–454, Feb. 2009.

[22] J.-S. Lee and E. Pottier, *Polarimetric Radar Imaging: From Basics to Applications.* Boca Raton, FL, USA: CRC Press, 2009.

[23] L. He, R. Panciera, M. A. Tanase, J. P. Walker, and Q. M. Qin, "Soil moisture retrieval in agricultural fields using adaptive model-based polarimetric decomposition of SAR data," *IEEE Trans. Geosci. Remote Sens.*, vol. 54, no. 8, pp. 4445–4460, Aug. 2016.

[24] H. Wang, R. Magagi, and K. Goïta, "Potential of a two-component polarimetric decomposition at C-band for soil moisture retrieval over agricultural fields," *Remote Sens. Environ.*, vol. 217, pp. 38–51, 2018.

[25] H. Wang, "Soil moisture retrieval from microwave remote sensing observations," in *Soil Moisture.* London, U.K.: IntechOpen, 2018.

[26] E. P. W. Attema and F. T. Ulaby, "Vegetation modeled as a water cloud," *Radio Sci.*, vol. 13, pp. 357–364, 1978.

[27] A. J. Graham and R. Harris, "Extracting biophysical parameters from remotely sensed radar data: A review of the water cloud model," *Prog. Phys. Geogr.*, vol. 27, no. 2, pp. 217–229, Jun. 2003.

[28] F. T. Ulaby, K. Sarabandi, K. Mcdonald, M. Whitt, and M. C. Dobson, "Michigan microwave canopy scattering model," *Int. J. Remote Sens.*, vol. 11, no. 7, pp. 1223–1253, 1988.

[29] R. D. De Roo, Y. Du, F. T. Ulaby, and M. C. Dobson, "A semi-empirical backscattering model at L-band and C-band for a soybean canopy with soil moisture inversion," *IEEE Trans. Geosci. Remote Sens.*, vol. 39, no. 4, pp. 864–872, Apr. 2001.

[30] S. S. Saatchi and M. Moghaddam, "Estimation of crown and stem water content and biomass of boreal forest using polarimetric SAR imagery," *IEEE Trans. Geosci. Remote Sens.*, vol. 38, no. 2, pp. 697–709, Mar. 2000.

[31] X. Huang, J. Wang, and J. Shang, "An integrated surface parameter inversion scheme over agricultural fields at early growing stages by means of C-band polarimetric RADARSAT-2 imagery," *IEEE Trans. Geosci. Remote Sens.*, vol. 54, no. 5, pp. 2510–2528, May 2016.

[32] W. T. An, Y. Cui, and J. Yang, "Three-component model-based decomposition for polarimetric SAR Data," *IEEE Trans. Geosci. Remote Sens.*, vol. 48, no. 6, pp. 2732–2739, Jun. 2010.

[33] G. C. Topp, J. L. Davis, and A. P. Annan, "Electromagnetic determination of soil water content: Application of TDR to field measurements," *Water Resources Res.*, vol. 16, pp. 574–582, 1980.

[34] M. C. Dobson, F. T. Ulaby, M. T. Hallikainen, and M. A. El-Rayes, "Microwave dielectric behavior of wet soil-Part II: Dielectric mixing models," *IEEE Trans. Geosci. Remote Sens.*, vol. GE-23, no. 1, pp. 35–46, Jan. 1985.

[35] J. L. Shang *et al.*, "Estimating plant area index for monitoring crop growth dynamics using Landsat-8 and RapidEye images," *J. Appl. Remote Sens.*, vol. 8, Nov./Dec. 2014, Art. no. 085196.

[36] S. R. Cloude and E. Pottier, "An entropy based classification scheme for land applications of polarimetric SAR," *IEEE Trans. Geosci. Remote Sens.*, vol. 35, no. 1, pp. 68–78, Jan. 1997.

[37] J. J. van Zyl, M. Arii, and Y. Kim, "Model-based decomposition of polarimetric SAR covariance matrices constrained for nonnegative eigenvalues," *IEEE Trans. Geosci. Remote Sens.*, vol. 49, no. 9, pp. 3452–3459, Sep. 2011.

[38] F. T. Ulaby, R. K. Moore, and A. K. Fung, *Microwave Remote Sensing: Active and Passive. Volume 2-Radar Remote Sensing and Surface Scattering and Emission Theory.* Boston, MA, USA: Addison-Wesley, 1982.

[39] J. Alvarez-Mozos, M. Gonzalez-Audicana, and J. Casali, "Evaluation of empirical and semi-empirical backscattering models for surface soil moisture estimation," *Can. J. Remote Sens.*, vol. 33, no. 3, pp. 176–188, Jun. 2007.

[40] Y. Kim, T. Jackson, R. Bindlish, S. Hong, G. Jung, and K. Lee, "Retrieval of wheat growth parameters with radar vegetation indices," *IEEE Geosci. Remote Sens. Lett.*, vol. 11, no. 4, pp. 808–812, Apr. 2014.

[41] N. Baghdadi *et al.*, "A potential use for the C-band polarimetric SAR parameters to characterize the soil surface over bare agriculture fields," *IEEE Trans. Geosci. Remote Sens.*, vol. 50, no. 10, pp. 3844–3858, Oct. 2012.
[42] Y. Yamaguchi, T. Moriyama, M. Ishido, and H. Yamada, "Four-component scattering model for polarimetric SAR image decomposition," *IEEE Trans. Geosci. Remote Sens.*, vol. 43, no. 8, pp. 1699–1706, Aug. 2005.
[43] M. S. Moran, L. Alonso, J. F. Moreno, M. Pilar Cendrero Mateo, D. Fernando de la Cruz, and A. Montoro, "A RADARSAT-2 quad-polarized time series for monitoring crop and soil conditions in Barrax, Spain," *IEEE Trans. Geosci. Remote Sens.*, vol. 50, no. 4, pp. 1057–1070, Apr. 2012.
[44] G. Di Martino, A. Iodice, A. Natale, and D. Riccio, "Polarimetric two-scale two-component model for the retrieval of soil moisture under moderate vegetation via L-Band SAR data," *IEEE Trans. Geosci. Remote Sens.*, vol. 54, no. 4, pp. 2470–2491, Apr. 2016.
[45] N. Baghdadi and M. Zribi, "Evaluation of radar backscatter models IEM, OH and Dubois using experimental observations," *Int. J. Remote Sens.*, vol. 27, no. 18, pp. 3831–3852, Sep. 2006.
[46] S. S. Wang, F. Q. Zhou, and H. A. J. Russell, "Estimating snow mass and peak river flows for the Mackenzie river basin using GRACE satellite observations," *Remote Sens.*, vol. 9, no. 3, Mar. 2017, Art. no. 256.
[47] D. F. Duan and Y. Wang, "An improved algorithm to delineate urban targets with model-based decomposition of PolSAR data," *Remote Sens.*, vol. 9, no. 10, Oct. 2017, Art. no. 1037.
[48] Q. H. Xie, J. D. Ballester-Berman, J. M. Lopez-Sanchez, J. J. Zhu, and C. C. Wang, "Quantitative analysis of polarimetric model-based decomposition methods," *Remote Sens.*, vol. 8, no. 12, pp. 1–4, Dec. 2016.
[49] A. Iodice, A. Natale, and D. Riccio, "Retrieval of soil surface parameters via a polarimetric two-scale model," *IEEE Trans. Geosci. Remote Sens.*, vol. 49, no. 7, pp. 2531–2547, Jul. 2011.

Tengfei Xiao received the B.S. degree in surveying and mapping from the Chengdu University of Technology, Chengdu, China, in 2018. He is currently working toward the M.S. degree in surveying and mapping from the University of Electronic Science and Technology of China, Chengdu.

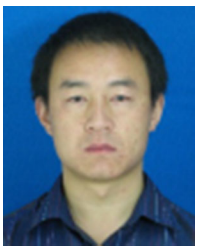

Minfeng Xing received the B.S. degree in electronic science and technology from Yunnan University, Kunming, China, in 2005, and the Ph.D. degree in remote sensing from the University of Electronic Science and Technology of China, Chengdu, China, in 2015.

He is currently an Associate Professor with the School of Environment and Resources, the University of Electronic Science and Technology of China. His research interests include the SAR image processing, the application of UAV, quantitative estimation of land surface variables from satellite remote sensing, and on integration of multiple data sources with numerical models.

Binbin He received the B.S. degree in resource exploration engineering and the M.S. degree in geology from the Chengdu University of Technology, Chengdu, China, in 1996 and 2002, respectively, and the Ph.D. degree in photogrammetry and remote sensing from China University of Mining and Technology, Xuzhou, China, in 2005.

He is currently a Professor with the School of Environment and Resources, the University of Electronic Science and Technology of China, Chengdu, China. His current research interests include quantitative estimation of land change from satellite remote sensing, and spatiotemporal data mining based on big data.

Jinfei Wang (Member, IEEE) received the B.S. and M.Sc. degrees from Peking University, Beijing, China, in 1982 and 1984, respectively, and the Ph.D. degree in geography from the University of Waterloo, Waterloo, ON, Canada, in 1989.

She is currently a Professor with the Department of Geography, the University of Western Ontario, London, ON, Canada. Her research interests include methods for information extraction from high resolution remotely sensed imagery, land use and land cover monitoring in urban environments and agricultural crop monitoring using multiplatform multispectral, hyperspectral, Lidar and radar data, and unmanned aerial vehicle data.

Jiali Shang (Member, IEEE) received the B.Sc. degree in geography from Beijing Normal University, Beijing, China, in 1984, the M.A. degree in geography from University of Windsor, Windsor, ON, Canada, in 1996, and the Ph.D. degree in environmental remote sensing from University of Waterloo, Waterloo, ON, Canada, in 2005.

She is currently a Research Scientist with the Ottawa Research and Development Centre of Agriculture and Agri-Food Canada and Adjunct Professor with York University, Toronto, ON, Canada, and Nipissing University, North Bay, ON, Canada. She has been actively involved in the methodology development and application of Earth observation (EO) technology to vegetation biophysical parameter retrieval, crop growth modeling, precision agriculture, and the detection of field operation activity related to crop production using both optical and radar EO data. In addition to conducting research, she has also been actively involved in student education, postdoc supervision, and international scientific collaborations.

Xiaodong Huang received the master's degree in photogrammetry and remote sensing from China University of Geosciences, Wuhan, China, in 2013, and the Ph.D. degree in geography from Western University Canada, London, ON, Canada, in 2016.

In 2017, he joined the Applied Geosolutions in United States as a Senior Research Scientist where he is currently leading the research and development program on application of Synthetic Aperture Radar Data for mapping and monitoring crop production. He has been involved in many NASA and USDA projects and is currently working on the development and validation of algorithms to be used for NASA-ISRO SAR (NISAR) mission's ecosystem products (focusing on cropland area). He also developed a SAR image processing tool named GITASAR to help SAR beginners to learn the SAR data processing in a simple way aiming to serve the SAR community. His research interests include the SAR signal and image processing, electromagnetic wave scattering over random media, and application of SAR, InSAR, and PolSAR technique to the soil moisture retrieval.

Xiliang Ni received the Ph.D. degree in cartography and geographic information systems from the Institute of Remote Sensing and Digital Earth, Chinese Academy of Sciences, Beijing, China, in 2013.

He is currently an Assistant Research Fellow with the Institute of Remote Sensing and Digital Earth, Chinese Academy of Sciences. His research interests include remote sensing of forest structure, biomass, carbon stock, and climate change.